Pump-Probe Spectroscopy of Population Wave Packets with Intense Chirped Pulses

JONATHAN SEGAL,[a] DAN HUPPERT,[a,*] AND BORIS D. FAINBERG[a,b]
[a]School of Chemistry, Raymond and Beverly Sackler Faculty of Exact Sciences, Tel Aviv University, Tel Aviv 69978, Israel
[b]Department of Exact Sciences, Holon Academic Institute of Technology, 52 Golomb Street, Holon 58102, Israel

(Received 21 September 2003 and in revised form 5 November 2003)

Abstract. We have studied the time evolution of population wave packets under intense chirped pulse excitation by resonance heterodyne optical Kerr effect spectroscopy. In general, this method enables us to obtain complementary information about population wave packets versus the absorption spectrum of an intense chirped pulse. We have generalized the "moving potentials" picture of one of the authors to a non-Debye solvent. We analyze the effects of both the parameters of the solvent–solute system and the electric field on the signal of the heterodyne optical Kerr effect experiment.

1. INTRODUCTION

Recent experiments on optical control involved the use of chirped pulses. The interaction of intense chirped ultrashort pulses with molecular systems in liquid solutions has shown that it is possible to control the ratio of the ground-state population to the excited population. The interaction of an intense pulse with a probe molecule in solution can be thought of in terms of sequential interactions with the field. In the nonlinear regime, more than one photon interacts with the molecular probe, and both absorption and stimulated emission can occur.

The effects of varying the chirp and intensity of an ultrashort pulse exciting probe molecules in liquid solutions have been investigated experimentally.[1–3] In these experiments the integrated fluorescence (which is directly proportional to the total excited-state population) after the completion of the pulse action was measured as a function of pulse chirp. In addition, the absorption spectrum of chirped pulses was measured.[1,3] For low-power excitation the absorption and the excited-state population were independent of chirp, while for high-power excitation the absorption exhibited a strong chirp dependence.

It has been shown in ref 4 that the absorption spectrum $\alpha_{abs}(\Omega)$ gives information about the population wave packet difference in the ground- and excited-electronic states $\Delta'(\omega_{21}-\omega(t),t)$ at the time moment t, when measured using strongly chirped pulses:

$$\alpha_{abs}(\Omega) \sim \Delta'(\omega_{21}-\omega(t),t) \qquad (1)$$

where $\omega(t)$ is the instantaneous pulse frequency, $\Omega = \omega(t)$, and ω_{21} is the frequency at the absorption band maximum.

Complimentary information about wave packets can be obtained using pump-probe spectroscopy with chirped both pump and probe pulses. By way of example, Apkarian et al.[5,6] have investigated by classical simulations the effect of linearly chirped pulses in ultrafast pump-probe experiments for the model system of I_2 isolated in a Kr matrix. They have shown that the chirp of the probe pulse can be used as a vectorial diagnostic of the momentum of the evolving wave packet. Their simulations and corresponding experimental results[7] concerned a *weak* excitation when the pump and probe pulses acted on different transitions.

In this paper, we are continuing our study of the time evolution of population wave packets under *intense* chirped pulse excitation.[4,8] We show that the resonance

*Author to whom correspondence should be addressed. E-mail: huppert@tulip.tau.ac.il

heterodyne optical Kerr effect (HOKE) spectroscopy with intense chirped pulses enables us in principal to obtain complementary information about population wave packets versus the absorption spectrum of an intense chirped pulse. The point is that the absorption spectrum directly reflects the time evolution of population wave packets' difference only at the configuration coordinate corresponding to instantaneous Franck–Condon transition at time t (see eq 1). In contrast, the resonance HOKE spectroscopy enables us to obtain similar information for any instantaneous Franck–Condon transition corresponding to time $t - \tau$, where τ is a variable delay between the pump and probe (or local oscillator, LO) pulses:

$$J_{HOKE}(\tau) \sim -\int_{-\infty}^{\infty} |E_{LO}(t-\tau)|^2 \Delta'^{NL}(\omega_{21} - \omega(t-\tau), t)dt \quad (2)$$

Here $\omega(t-\tau)$ is the instantaneous LO (or probe) frequency, $\Delta'^{NL}(\omega_{21} - \omega(t-\tau),t)$ is the deviation of $\Delta'(\omega_{21} - \omega(t-\tau),t)$ from its equilibrium value at the configuration coordinate corresponding to instantaneous Franck–Condon transition at time $t - \tau$, and $E_{LO}(t-\tau)$ is the LO field amplitude.* In other words, the HOKE spectroscopy enables us to obtain information about the population wave packet difference for *any* τ, i.e., for the values of the configuration coordinate corresponding to instantaneous Franck–Condon transitions for different frequencies $\omega(t-\tau)$ (not only for $\omega(t)$ as in the absorption spectrum measurements).

The remainder of this paper is organized as follows: In Section 2, we calculate signals in the transmission "pump-probe" and HOKE experiments. In Section 3, the setup of the HOKE experiments is depicted. In Section 4, we analyze numerically the effects of the parameters of the solvent–solute system and of the electric field on the signal of the HOKE experiments. We also fit the results of the model to the experimental results. A summary of the numerical and the experimental results is given in the last section. In the Appendix the nonperturbative model, which is used for our analysis, is extended to the non-Debye solvent environment. There we generalize the theory of refs 9,10 to the relaxation in non-Debye solvent.

2. THEORY

In the transmission "pump-probe" experiment[11–13] a second pulse (whose duration is the same as the pump pulse) probes the sample transmission ΔT at a delay τ. This dependence $\Delta T(\tau)$ is given by[14]

$$\Delta T(\tau) \sim -\omega Im \int_{-\infty}^{\infty} E_{pr}^{*}(t-\tau) P^{NL+}(t)dt \quad (3)$$

where E_{pr} and $P^{NL+}(t)$ are the amplitudes of the positive frequency component of the probe field and the nonlinear polarization, respectively.

In a resonance HOKE spectroscopy[15–17] (see Fig. 1), a linearly polarized pump pulse at frequency ω induces anisotropy in an isotropic sample. After the passage of the pump pulse through the sample, a linearly polarized probe pulse at $\pi/4$ rad from the pump field polarization, is incident on the sample. A polarization analyzer is placed after the sample oriented at approximately $\pi/2$ (but not exactly) with respect to the probe pulse polarization. A small portion of the probe pulse that is not related to the induced anisotropy plays the role of a local oscillator (LO) with a controlled magnitude and phase.

The HOKE signal can be written in the form:[18]

$$J_{HOKE}(\tau) \sim -Im \int_{-\infty}^{\infty} E_{LO}^{*}(t-\tau) \exp(i\psi) P^{NL+}(t)\, dt \quad (4)$$

where ψ is the phase of the LO. If $\psi = \pi/2$, the resonance HOKE spectroscopy provides information about the real part of the nonlinear susceptibility (the change in the index of refraction). If $\psi = 0$, the resonance HOKE spectroscopy provides information similar to that of the transmission pump-probe spectroscopy (see eq 3). Therefore, we will discuss for brevity only the HOKE spectroscopy for $\psi = 0$, bearing in mind that all our results are also true for the transmission "pump-probe" experiment.

We will calculate the signal $J_{HOKE}(\tau)$ of a resonance HOKE spectroscopy of a solute molecule in a solvent with both chirped intense pump and a weak LO. The LO is a copy of pump, and probes the sample-induced anisotropy at a delay τ. By way of analogy with ref 10, consider a molecule with two electronic states $n = 1$ and 2 in a solvent described by the Hamiltonian

$$H_0 = \sum_{n=1}^{2} |n\rangle \left[E_n + W_n(\mathbf{Q})\right] \langle n| \quad (5)$$

where $E_2 > E_1$, E_n is the energy of state n and $W_n(\mathbf{Q})$ the adiabatic Hamiltonian of reservoir R (the vibrational subsystems of a molecule and solvent interacting with the two-level electron system under consideration in state n). The molecule is affected by electromagnetic radiation of a number of beams

$$\mathbf{E}(t) = \mathbf{E}^{+}(t) + \mathbf{E}^{-}(t) = \frac{1}{2}\sum_{m} \vec{E}_m(t) \exp(-i\omega_m t) + c.c. \quad (6)$$

For phase-modulated pulses, the field amplitudes $\vec{E}_m(t)$ can be presented by

$$E_m(t) = \mathcal{E}_m(t) \exp(i\varphi_m(t)) \quad (7)$$

where $\varphi_m(t)$ describes the change of the pulse phase in time t.

Since the absorption spectrum of a large molecule in

*Eq 2 is a special case of the more general eq 14 (see below) in the absence of the optically active high-frequency intramolecular vibrations.

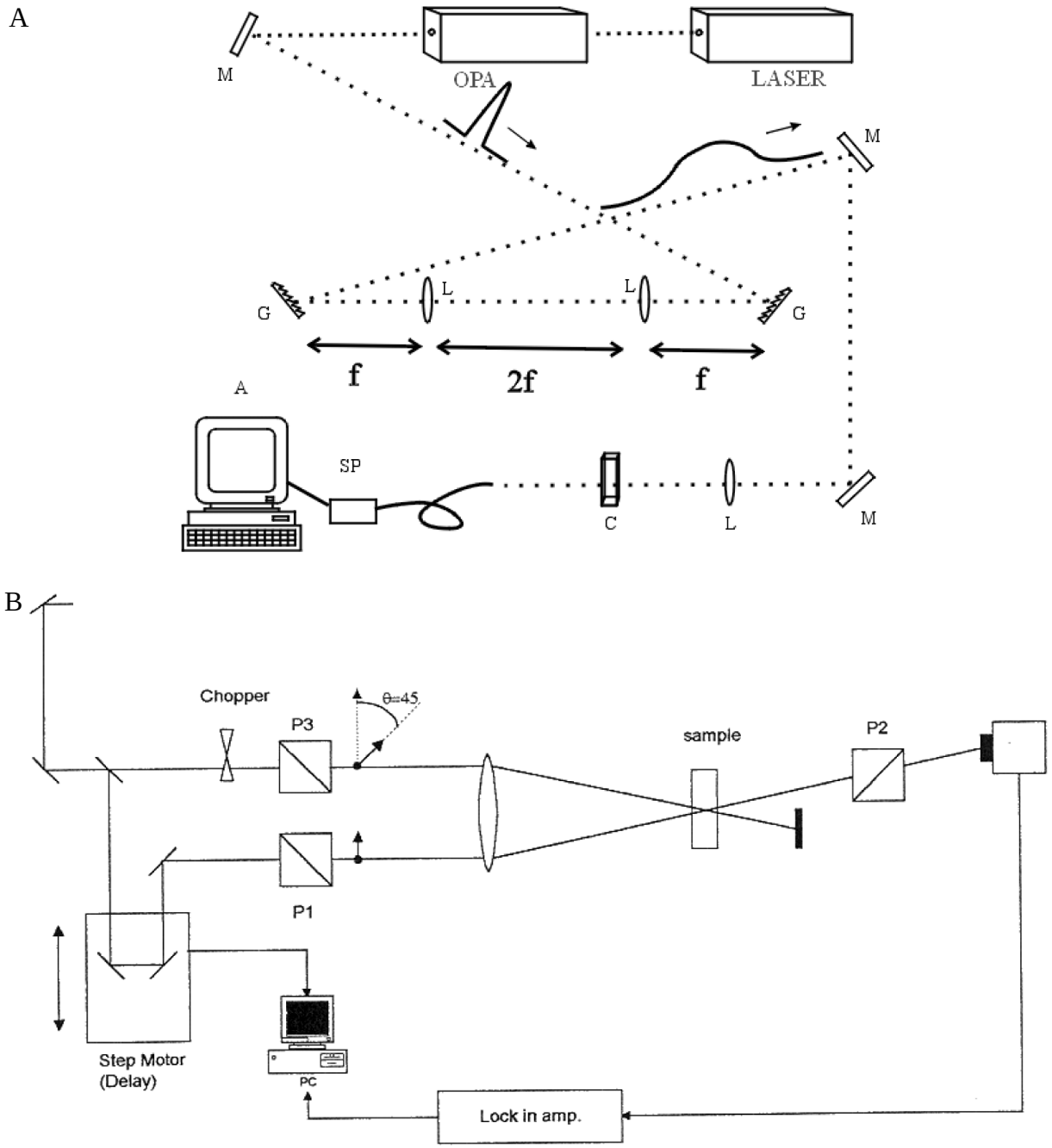

Fig. 1. Experimental setup—(a) Two-gratings compressor for generating linear chirped pulses. The left grating is moved parallel to the lenses' optical axis for controlling the pulse's chirp. Captions: M—mirror, L—lens, G—grating. (b) OKE autocorrelator. Captions: P—polarizer, BS—beamsplitter, D—detector, short lines—mirrors.

solution consists of overlapping vibronic transitions, we shall single out the contribution from low frequency (LF) optically active (OA) vibrations, $\{\omega_s\}$, to $W_n(\mathbf{Q})$: $W_n(\mathbf{Q}) = W_{nM} + W_{ns}$ where W_{ns} is the sum of the Hamiltonian governing the nuclear degrees of freedom of the solvent in the absence of the solute and LFOA intramolecular vibrations, and the part which describes interactions between the solute and the nuclear degrees of freedom of the solvent; W_{nM} is the Hamiltonian representing the nuclear degrees of freedom of the high-frequency (HF) OA vibrations of the solute molecule.

Electromagnetic field (eq 6) induces an optical polarization in the medium $\mathbf{P}(t)$ which can be expanded in powers of $\mathbf{E}(t)$:[19]

$$\mathbf{P}^{(n)}(t) = NTr_R\,(\mathbf{D}\rho^{(n)}(t)) \tag{8}$$

where N is the density of particles in the system; **D** is the dipole moment operator of a solute molecule; $\rho^{(n)}$ is the density matrix of the system calculated in nth approximation with respect to $\mathbf{E}(t)$.

We consider only resonance light–matter interactions. We assume that a strong pump $1/2\vec{E}(t)\exp(-i\omega t) + c.c.$ acts at the electronic transition $1 \rightarrow 2$, and a weak probe resonance $1/2\vec{E}_{pr}(t-\tau)\exp[-i(t-\tau)\omega] + c.c.$ field delayed by a variable τ acts at the same transition and does not overlap in time with the pump, i.e.,

$$\sum_m \vec{E}_m(t)\exp(-i\omega_m t) = \vec{E}(t)\exp(-i\omega t) + \vec{E}_{pr}(t-\tau)\exp[-i(t-\tau)\omega]$$

The density matrix satisfies the Liouville equation:

$$i\hbar\frac{\partial\rho}{\partial t} = [H_0 + H'(t), \rho] \tag{9}$$

where $H'(t) = -\mathbf{DE}(t)$.

Consider first the contributions from the LFOA vibrations $\{\omega_s\}$. In the case of appreciable Stokes losses when the perturbation of the nuclear system under electronic excitation $1 \rightarrow 2$ (a quantity $V_s = W_{2s} - W_{1s}$) is large, one can use a semiclassical (short time) approximation.[20] It corresponds to the fast electronic dephasing limit. In the last case one can consider the density matrix diagonal with respect to electronic indices $\rho_{nn}(t)$. In the presence of OA intramolecular vibrational modes, one ought to consider the density matrix averaged with respect to these modes:[10]

$$\rho_{ns}(t) = Tr_M\,\rho_{nn}(t) \tag{10}$$

where the total density matrix $\rho_{nn}(t)$ is factorized

$$\rho_{nn}(t) = \rho_{nM}\,\rho_{ns}(t) \tag{11}$$

and

$$\rho_{nM} = \exp(-\beta W_{nM})/Tr_M\exp(-\beta W_{nM})$$

is the equilibrium density matrix of the intramolecular OAHF vibrations. Here Tr_M denotes the operation of taking a trace over the variables of the intramolecular OAHF vibrations, $\beta = 1/(k_BT)$.

When the contribution from LFOA vibrations is described as the Gaussian–Markovian stochastic modulation of the electronic transition, the density matrix $\rho_{ns}(t)$ can be presented as a function of the generalized coordinate α: $\tilde{\rho}_{ns}(\alpha,t)$.[10] Knowing the density matrix $\tilde{\rho}_{ns}(\alpha,t)$, one can calculate the amplitude of the positive frequency component of the polarization $P^+(t)$ by equation 12 of ref 8 and taking into account only the linear changes of the field phase during time τ:[9]

$$P^+(t) = \frac{iN|D_{12}|^2}{2\hbar}\mathcal{E}_{pr}(t-\tau)\int_{-\infty}^{\infty}d\alpha\int_0^{\infty}d\tau' \times \exp[i(\omega(t-\tau)-\omega_{21}+\alpha)\tau'] \times \{f^*_{\alpha M}(\tau')\tilde{\rho}_{1s}(\alpha,t) - f^*_{\varphi M}(\tau')\tilde{\rho}_{2s}(\alpha,t)\} \tag{12}$$

where $\omega(t) = \omega - d\varphi/dt$, and

$$f_{\alpha,\varphi M}(\tau') = Tr_M[\exp(\pm(i/\hbar)W_{2,1M}\tau')\exp(\mp(i/\hbar)W_{1,2M}\tau')\rho_{1,2M}] \tag{13}$$

are the characteristic functions (the Fourier transforms) of the "intramolecular" absorption (α) or emission (φ) spectrum.[20]

Substituting the last equation into eq 4, we obtain for $\psi = 0$

$$J_{HOKE}(\tau) \sim -\frac{N|D_{12}|^2}{2\hbar}\int_{-\infty}^{\infty}dt|E_{LO}(t-\tau)|^2 \times \mathrm{Re}\int_0^{\infty}d\tau'\int_{-\infty}^{\infty}d\alpha\exp[i(\omega(t-\tau)-\omega_{21}+\alpha)\tau'] \times \{f^*_{\alpha M}(\tau')\tilde{\rho}^{NL}_{1s}(\alpha,t) - f^*_{\varphi M}(\tau')\tilde{\rho}^{NL}_{2s}(\alpha,t)\} \tag{14}$$

where $\tilde{\rho}^{NL}_{ns}(\alpha, t)$ are the deviations of $\tilde{\rho}_{ns}(\alpha,t)$ from its equilibrium value

$$\tilde{\rho}^{(0)}_{ns}(\alpha) = (2\pi\sigma_{2s})^{-1/2}\exp[-\alpha^2/(2\sigma_{2s})] \tag{15}$$

$\sigma_{2s} = \omega_{st}k_BT/\hbar$, ω_{st} is the Stokes shift of the equilibrium absorption and luminescence spectra.

Let us consider one normal intramolecular oscillator of frequency ω_0 whose equilibrium position is shifted by ΔQ under electronic transition. Its characteristic functions $f_{\alpha,\varphi M}(\tau')$ are determined by the following expression:[21]

$$f_{\alpha,\varphi M}(\tau') = \exp(-S_0\coth\theta_0) \times \sum_{k=-\infty}^{\infty} I_k(S_0/\sinh\theta_0)\exp[k(\theta_0 \pm i\omega_0\tau')] \tag{16}$$

where S_0 is the Huang–Rhys factor[37] defined by $S_0 = \omega_0(\Delta Q)^2/(2\ h)$, $\theta_0 = h\omega_0/(2k_BT)$, $I_n(x)$ is the modified Bessel function of the first kind.[22] Substituting this expression into eq 14, we obtain

$$J_{HOKE}(\tau) \sim -\exp(-S_0\coth\theta_0) \times \sum_{k=-\infty}^{\infty} I_k(S_0/\sinh\theta_0)\exp(k\theta_0) \times \int_{-\infty}^{\infty}dt|\mathcal{E}_{LO}(t-\tau)|^2 \times \{\tilde{\rho}^{NL}_{1s}[\omega_{21} - \omega(t-\tau) + k\omega_0, t] - \tilde{\rho}^{NL}_{2s}[\omega_{21} - \omega(t-\tau) - k\omega_0, t]\} \tag{17}$$

If quantum intramolecular modes are of a high frequency, so that $\hbar\omega_0 \gg k_B T$, eq 17 is reduced to**

$$J_{HOKE}(\tau) \sim -\exp(-S_0)\sum_{k=0}^{\infty}\frac{S_0^k}{k!}$$
$$\times\int_{-\infty}^{\infty} dt|\mathcal{E}_{LO}(t-\tau)|^2\{\tilde{\rho}_{1s}^{NL}[\omega_{21}-\omega(t-\tau)+k\omega_0,t]$$
$$-\tilde{\rho}_{2s}^{NL}[\omega_{21}-\omega(t-\tau)-k\omega_0,t]\} \qquad (18)$$

The population wave packets $\tilde{\rho}_{2s}$ $[\omega_{21}-\omega(t-\tau)-(-1)^n k\omega_0, t]$ can be found by solving equation 42 of ref 10. The extension of the theory to non-Debye solvents is carried out in the Appendix.

3. EXPERIMENTAL SETUP

The optical experimental setup consists of a femtosecond laser source, an optical parametric amplifier (OPA), a pulse-shaping device, and a setup for measurement of the resonance HOKE signal. The laser system consists of a Ti:Sapphire-based oscillator (Mira Seed Coherent) and a multipass-based Ti:Sapphire amplifier (Quantronix Odin), which produces laser pulses of 40 fs duration, centered near 800 nm, with a pulse energy of 600 μJ and a repetition rate of 1 kHz. These pulses are used to pump an OPA that generates tunable short intense and coherent pulses of 50 fs with 25-nm bandwidth in the spectral range of 600–770 nm. The pulse-shaping apparatus consists of a pair of 600 lines/mm gratings and two identical lenses with focal length of f = 15 cm. Their layout is shown in Fig. 1a. By moving one of the gratings collinearly with the optical axis, the pulse gains positive or negative linear chirp.[23] The chirp sign depends on the direction of the movements with respect to the lens focus. During the experiments, two chirp rates were chosen, –50000 and 50000 fs^2, hereafter negative and positive chirp rate, respectively. The pulse temporal shape was diagnosed by an OKE (optical Kerr effect) autocorrelator for determining the pulse chirp.[24] The sample is irradiated by 10-μJ pulses, focused by a 15-cm lens. The cell was placed about 2 cm from the focus (the spot size was 360 µm at the sample) to avoid other nonlinear effects. Neutral density filters attenuated the pulse intensity. In the experiments, we use Rhodamine 800 dye (R800) and DTTCI (3,3′-diethylthiacarbocyanine iodide), which were purchased from Exciton, in 1-mm or 0.2-mm quartz cells. The dyes are dissolved in methanol. The optical density of the solution was about 0.7. In the time-resolved resonance HOKE experiment, the laser-induced anisotropy created by the resonant absorption of the pump pulse photons is probed by a variably delayed, weak, polarized probe pulse. The change in the polarization state of the probe beam was detected by the transmission through a crossed polarizer pair (P1 and P2 in Fig. 1b) of the probe beam as a function of the time delay between the pump and the probe pulses. In order to amplify the optical Kerr signal, and avoid complexity due to the quadratic nature of the signal, we used heterodyne methods for signal detection. A local oscillator was derived by minor rotation of the analyzer polarizer (P2) by <1° from the maximum extinction position part of the probe pulse, which is in phase, and polarized orthogonally to the probe polarization. The magnitude of the local oscillator intensity is about 30 times larger than that of the Kerr signal. The use of a local oscillator with field $\mathcal{E}_{LO}$ and light intensity I_{LO} to detect a signal with a field $\mathcal{E}_s$ and intensity I_s results in a detector response of:

$$I_{LO} + I_s + \frac{nc}{8\pi}\left(\mathcal{E}_s^*\mathcal{E}_{LO} + \mathcal{E}_{LO}^*\mathcal{E}_s\right) \qquad (19)$$

The crossed term in parenthesis is the heterodyne term.

4. RESULTS AND DISCUSSION

We measured the effect of both the chirp rate and intensity of the ultrafast pump laser pulse on the HOKE signal of large dye molecules in polar liquids. The resonance HOKE signal for $\psi = 0$ provides information similar to that of traditional pump-probe experiment signals. An advantage of the HOKE signal is that it is a null technique where, prior to the pump excitation, no light passes through the analyzer (polarizer P2 in Fig. 1b). In the absence of high-frequency optically active vibrations, the signal is directly related to the time-dependent deviation of the population difference between the ground and excited state from its equilibrium value $\Delta'^{NL}(\omega_{21}-\omega(t-\tau),t)$ (see eq 2).

Prior to presenting our experimental results, we will first present our model simulations of the effects of the pump, probe, and the solvent–solute system properties on the resonance HOKE signal. We solved equation 42 of ref 10 numerically. The diffusion equation computer program is based on the Kosloff–Tal-Ezer time propagator in a Chebyshev polynomial expansion.[25] The computer routine calculates the populations as a function of the coordinate and time, and then calculates the HOKE signal by using eq 18.

A. The Effects of the Pump

Two parameters that characterize the pump pulse are (1) the chirp rate and (2) the intensity of the pulse.

1. The chirp rate. The calculated OKE signals, as a function of time at various chirp rates of the pulse, are

**Strictly speaking, eqs 2, 14, 17, 18, and eqs A7, A9 below are correct only for non-overlapping pump and probe pulses. However, for strongly chirped both pump and probe this criterion is much weaker. The point is that for delays of the order of pulse duration, in spite of overlapping the pump and probe pulses, repumping the pump into the probe is very small. This is due to relatively large differences of the pump and probe instantaneous frequencies for the delays under consideration. Therefore, eqs 2, 14, 17, 18, and eqs A7, A9 are incorrect only for very small delays, which are much smaller than pulse duration. A contribution of this time interval into the signal is negligible.

depicted in Figs. 2a and 2b. The amount of population transferred from the excited state to the ground state depends on the synchronization of the chirp rate and the solvent relaxation, since a momentary population inversion is achieved. Maximum population transfer will occur at a certain chirp rate that corresponds to the best match with the solvent coordinate relaxation time τ_s. In the case that results in negligible dump, or the case of positively chirped pulses, the chirp affects the buildup of both "holes" and "particles" population profiles. Again, the synchronization between solvent relaxation time τ_s and chirp rate has a profound effect on the effectiveness of the dump process.

In contrast to a positively chirped pulse excitation, for a negatively chirped pulse, the population reaches the equilibrium position (the bottom of the potential well of the excited state) faster, and hence the build up of the OKE signal for a negatively chirped pulse is faster than that for positively chirped pulses (as seen from Figs. 2a and 2b).

2. The intensity of the pulse. For negatively chirped pulses, the intensity of the pump pulse determines the effectiveness of the dump process. In general, the larger the pulse intensity, the larger the OKE signal, since the sum of "holes" and "particles" at the relevant coordinates is larger (excluding saturation effects). For positively chirped pulses, the shape of the normalized OKE signal does not depend on the pump pulse intensity. This finding arises from the fact that the amount of population raised to the excited state is proportional to the pulse intensity.

Unlike the positively chirped pulse excitation, for a negatively chirped pulse under effective dump "conditions", the shape of the normalized OKE signals strongly depends on the pump pulse intensity. This is explained by the fact that the amount of the transferred population (from the excited state to the ground state) depends not only on the laser intensity but also on the total population of the state, which was previously transferred from the ground state. In the case of a "dump" process, the "blue part" of the pulse transfers the population to the excited state, which is proportional to the total population in the ground electronic state. The "red part" of the pulse transfers the population from the excited state back to the ground state in proportion to the excited state population. Thus, the overall process of population transfer is nonlinear.

B. The Effects of the Probe

The probe pulse intensity is weak and hence does not influence the population. The OKE signal depends on the probe pulse chirp and its carrier frequency only. The dependence of the OKE signals on the carrier frequency shows a distinct effect. The influence of the solvent relaxation on this dependence will be discussed later. As seen in Figs. 2a and 2b, the chirp determines the pulse width, and therefore the OKE signal rise time increases with the increase in the chirp. Also, the dynamics of the OKE signal slows down as the chirp increases, since the population transfer rate also decreases as the chirp increases. In addition, the probe monitors the changes at a slower rate.

C. The Effects of the Solvent–Solute System Properties

In addition to the dependence of the OKE on both the pump and probe pulse parameters, the OKE signal also depends on the probe molecule and solvent bath properties. The molecular parameters are the correlation time τ_s, the Stokes shift ω_{st}, the molecule oscillator strength,

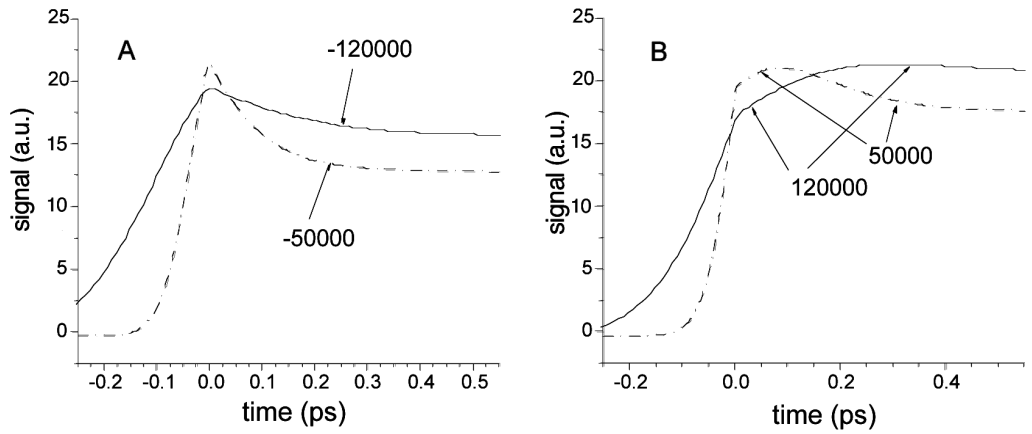

Fig. 2. Simulations of OKE signals of DTTCI as functions of the pulses chirp ($|\Phi''(\nu)|$ = 50000,120000 fs^2). Fig. 2a is for the negative chirps and Fig. 2b is for the positive chirps. Transform-limited pulse temporal width is equal to 30 fs, τ_s = 50 fs, the central excitation wavelength = 770 nm, ω_{st} = 800 cm^{-1}, and the intensity factor Q' (see ref 9) is equal to 2.

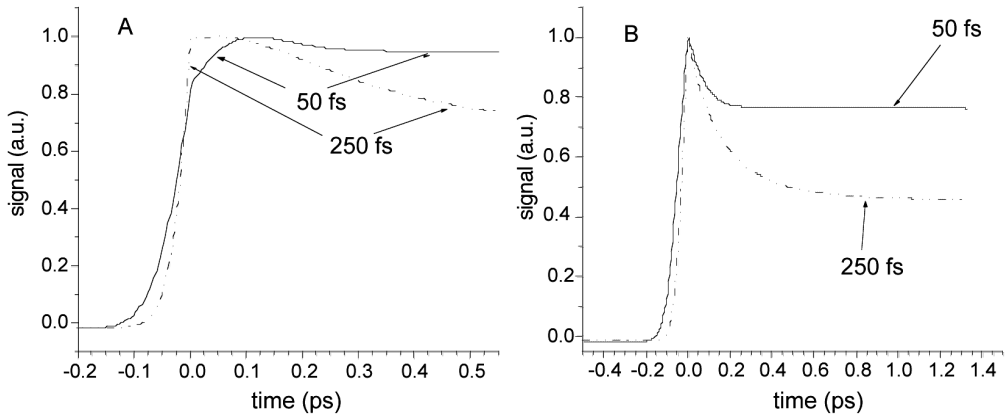

Fig. 3. Simulations of OKE signals in DTTCI as a function of the relaxation time (τ_s = 50,250 fs). Figure 3A is for the positive chirp: 50000 fs^2 and Fig. 3B is for the negative chirp: –50000 fs^2. The rest of the parameters are the same as in Fig. 2.

the frequency of the OAHF vibrations ω_0, and S_0 (the Huang–Rhys factor). We obtained the last four parameters from the fit of the experimental absorption or emission spectrum to equation 35 of ref 8. Figures 3a and 3b show the dependence of the calculated OKE signal on τ_s for $\Phi''(\nu)$ = 50000 fs^2 and –50000 fs^2, respectively. The calculation is for DTTCI dye in methanol, where the laser carrier wavelength is 770 nm and the absorption band maximum is at 760 nm. For negatively chirped pulse, the relative amplitude of the long-time behavior of the signal depends on τ_s. The longer the relaxation time, the larger is the amplitude of

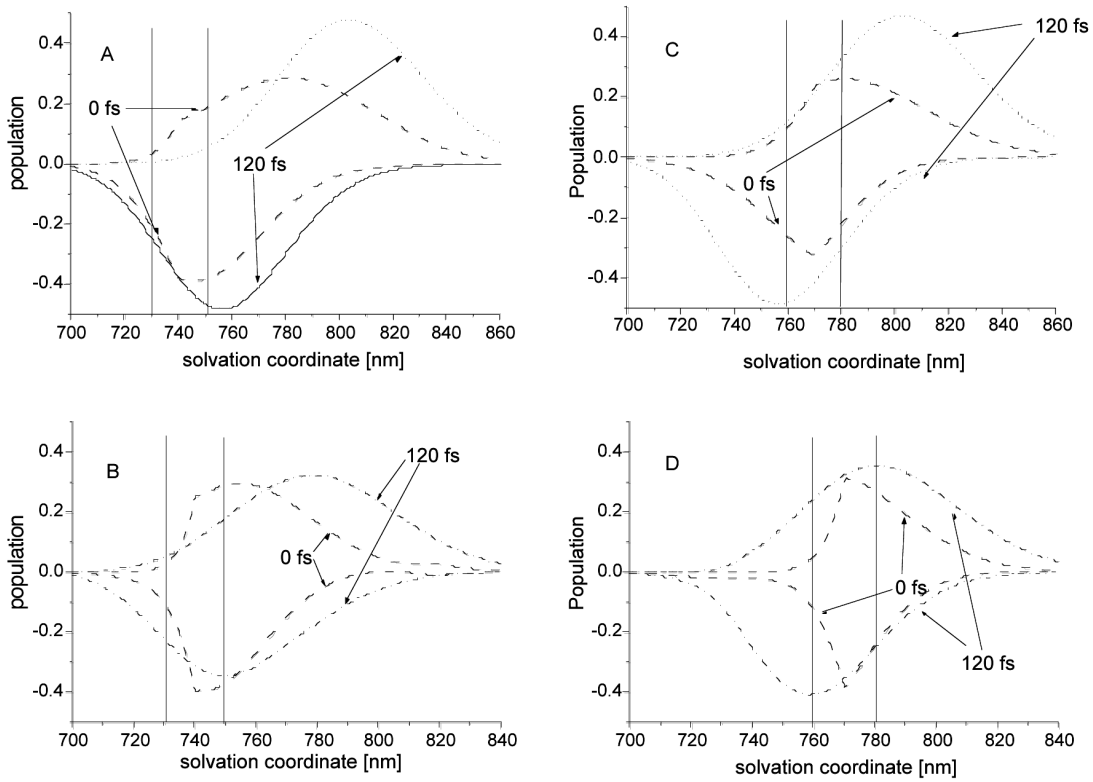

Fig. 4. Simulation of the population wave packets of the particles and holes as a function of the delay time from the peak of the pump pulse (0 fs and 120 fs). Vertical lines limit the frequency window of the probe pulse. The pump and probe central wavelengths are 740 nm (Figs. 4a and 4b) and 770 nm (Figs. 4c and 4d). τ_s = 50 fs (Figs. 4a and 4c) and 250 fs (Figs. 4b and 4d). The rest of the parameters are the same as in Fig. 2.

the decay. The latter behavior can be explained by an efficient dump process for slow relaxation. For a positively chirped pulse, when τ_s is short, we see a rise of the OKE signal (up to 100 fs), followed by a signal decrease. For longer solvent relaxation times, the OKE signal immediately decreases for positive delay times. The explanation of this observation is given below. The dynamics of the prepared nonequilibrium population wave packet is seen in Figs. 4a–4d. We use a transformation of the abscissa from a generalized solvent coordinate to wavelength coordinate. The transition frequency is given by:

$$\nu(\alpha) = \frac{U_2(\alpha) - U_1(\alpha)}{h} \tag{20}$$

$$\lambda(\alpha) = c/\nu(\alpha) \tag{21}$$

where the effective parabolic potentials $U_{1,2}(\alpha)$ are determined by equation 12 of ref 9, c is the speed of light. Figures 4a and 4b display the population wave packets excited and measured near 740 nm, and Figs. 4c and 4d, near 770 nm. The correlation times are τ_s = 50 fs (for Figs. 4a and 4c) and 250 fs (for Figs. 4b and 4d). As seen, there is a strong dependence of the obtained signals on the pump and probe laser wavelengths. Figures 5a–5c show the effect of the central laser wavelength on the HOKE signal for various relaxation times and positive chirp ($\Phi''(\nu)$ = 50000 fs^2). The excitation wavelength has a distinct effect on the shape of the normalized OKE signal. As seen in Figs. 5a–5c, for long-wavelength excitation, a rise time of the signal is noticeable. The maximum of the OKE signal appears at a time τ_{peak} after the excitation. The shorter the excitation wavelength, the shorter is τ_{peak}. At a certain short wavelength, τ_{peak} is close to zero and the OKE signal reaches a maximum (at pulse convolution) and then decays with a time constant that depends on the excitation wavelength. The shorter the excitation, the longer is the decay time. For large τ_s, the amplitude of the rise time component decreases.

For negatively chirped pulses, the effect of the pump's wavelength on the shape of the OKE signal is small (almost negligible).

D. Experimental Data

We used our computer program based on the theory given in the previous section and the experimental pa-

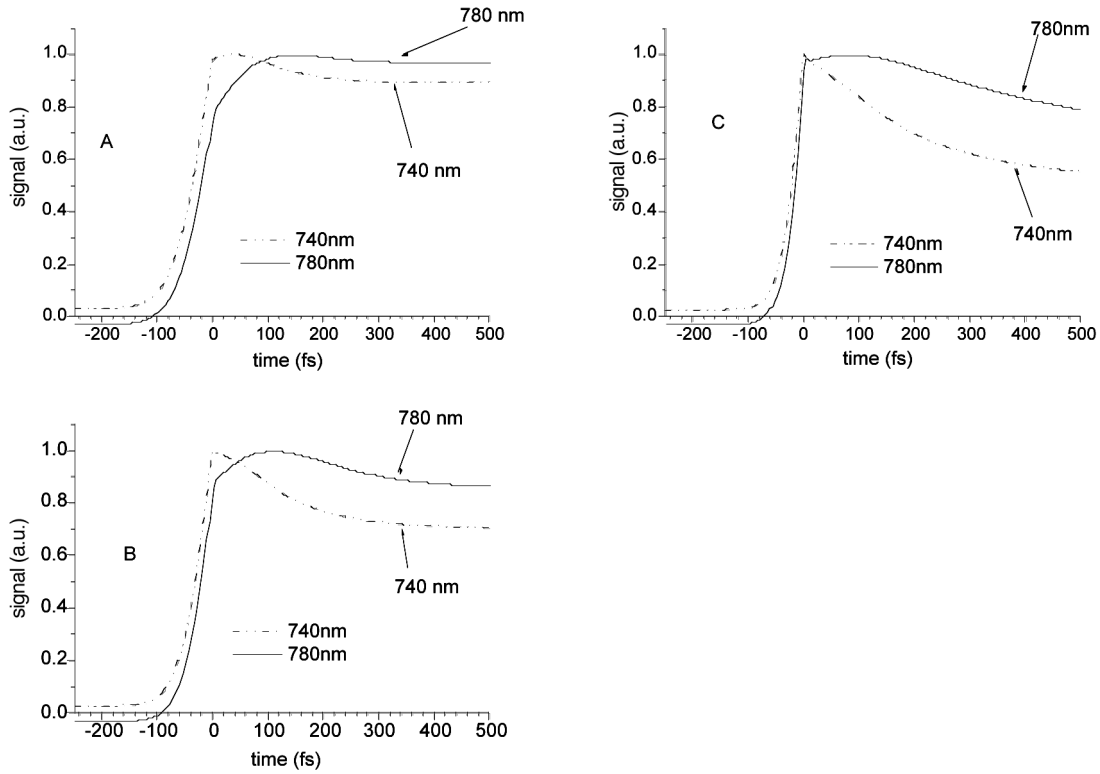

Fig. 5. Simulation of OKE signals of DTTCI for positive chirp ($|\Phi''(\nu)|$ = 50000 fs^2) and various central wavelengths of the pump and probe (740, 780 nm). τ_s = 50 (5a), 100 (5b), and 250 fs (5c), respectively. The rest of the parameters are the same as in Fig. 2.

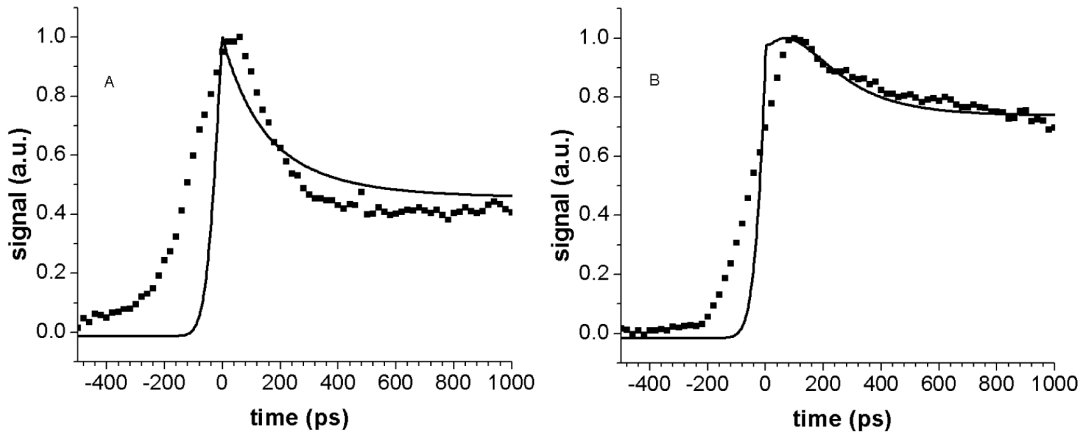

FIG. 6. Experimental results (markers) of the OKE signals of DTTCI/MeOH for a negatively chirped pulse (–50000 fs^2) (Fig. 6a) and positively chirped pulse (50000 fs^2) (Fig. 6b). The solid lines are the theoretical fits. The correlation time τ_s used for the fit of (a) τ_s = 170 fs; for (b) τ_s = 250 fs. Central excitation wavelength = 640 nm, ω_{st} = 618 cm^{-1}, Q' = 1.

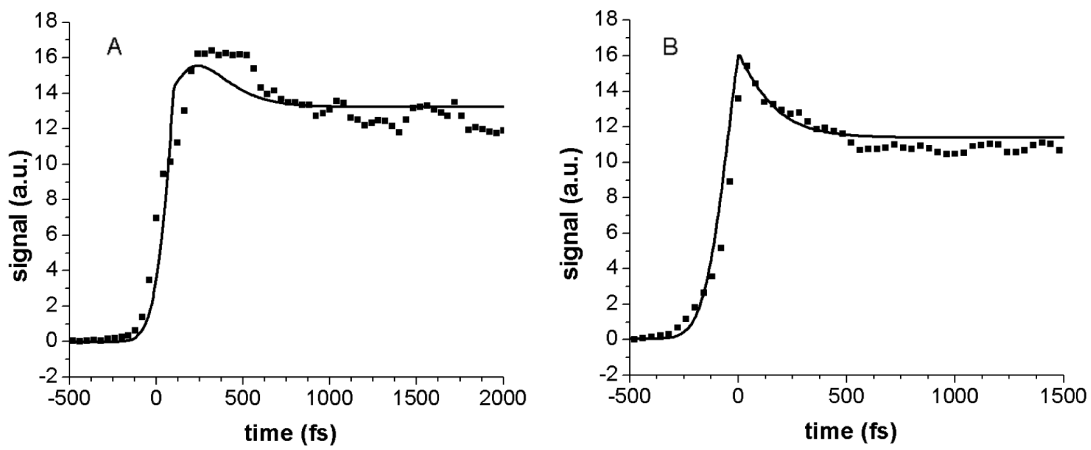

Fig. 7. Experimental results (markers) of the OKE signals of Rh800/MeOH for a positively chirped pulse (50000 fs^2) (Fig. 7a) and for negatively chirped pulse (–50000 fs^2) (Fig. 7b). Solid lines are the theoretical fits. Transform-limited pulse temporal width is equal to 35 fs, correlation time τ_s = 150 fs, central excitation wavelength = 680 nm, ω_{st} = 800 cm^{-1}, the saturation parameter (see ref 9) Q' = 1, ω_0 = 1300 cm^{-1}, S_0 = 0.45.

rameters to fit both positively and negatively chirped HOKE signals of DTTCI, shown in Fig. 6, and Rhodamine-800 in methanol, shown in Fig. 7. As seen from the experimental OKE signal of Rhodamine 800, the computed fit is rather good, while our fit to the DTTCI data is somewhat less good. A possible explanation for this is the asymmetric spectral profile of the fundamental wavelength (800 nm), which was used for DTTCI.

The laser pulse parameters used to fit the signals, shown in Fig. 7, are: λ_0 = 680 nm, the central laser wavelength, Q' = 1 (the saturation parameter (see ref 9), Φ'' (v) = +50000 and –50000 fs^2. The ground- and excited-states potential surfaces were constructed from both the absorption band and emission band positions and shapes. For the best fit of the experimental results we found that the short component of the solvation τ_s, τ_s = 150 fs.

The corresponding wave packets of both the excited and ground states of various times are shown in Fig. 8. At short times and at low laser pulse intensity, both the excited- and ground-state wave packets are of Gaussian shape, whose width is determined by the laser pulse spectral bandwidth. The position on the potential surface

of the initial wave packets depends on the detuning of the laser frequency with respect to the frequency of the Franck–Condon transition. As time progresses, both excited- and ground-state wave packets reach the equilibrium positions on the potential surfaces. The initial relatively narrow bandwidth of the wave packets increases as the time progresses and finally reaches the equilibrium width.

As described before, in the case of intense short laser pulses, population can be transferred not only from the ground state to the excited state, but also from the excited state back to the ground state. These processes occur effectively in the case of intense negatively chirped pulses.

As seen in Fig. 4, the wave packet population of both ground and excited states differ strongly between positively and negatively chirped pulses. This is a consequence of the efficient dump process of population from the excited state to the ground state when the sample is excited by a negatively chirped pulse. This phenomenon and carefully selected laser center wavelength and chirp rate and intensity enable us to control both the ground and excited wave packets of large dye molecules in the condensed phase.

5. SUMMARY

In this work we studied the time evolution of population wave packets under intense chirped pulse excitation by the resonance HOKE spectroscopy with intense chirped pulses. In general, the last method enables us to obtain complementary information about population wave packets versus the absorption spectrum of an intense chirped pulse.

We analyzed the effects of both the parameters of the solvent–solute system and the electric field on the signal on the HOKE experiment. We fitted the results of the model to the experimental results, which correlate well. Such a fitting enables us to obtain a time evolution of population wave packets under intense chirped pulse excitation.

Acknowledgments. This research was supported by the Israel Science Foundation (grant no. 41/00-1) and the James Franck Binational German-Israel Program in Laser Matter Interaction.

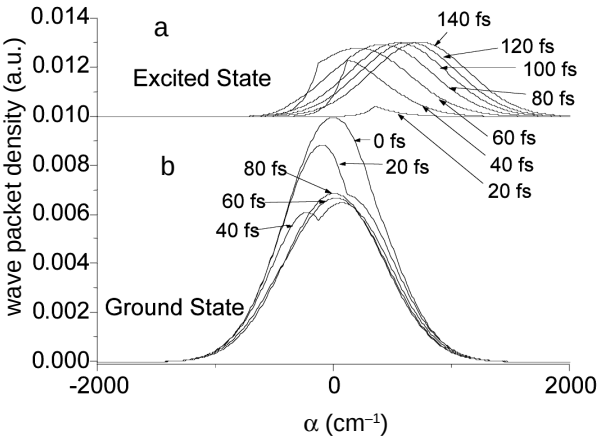

Fig. 8. Population wave packet dynamics (in steps of 20 fs) in Rh800/MeOH for the excited state (Fig. 8a) and for the ground state (Fig. 8b) found by fitting experimental results of Fig. 7. Transform-limited pulse temporal width = 35 fs, correlation time τ_s = 150 fs, central excitation wavelength = 680 nm, ω_{st} = 800 cm^{-1}, saturation parameter (see ref 9) Q' = 1, ω_0 = 1300 cm^{-1}, S_0 = 0.45, chirp = 50000 fs^2.

APPENDIX: EQUATIONS FOR POPULATION WAVE PACKETS FOR NON-DEBYE SOLVENT IN THE PRESENCE OF INTRAMOLECULAR MODES

A signal in a pump-probe and in a resonance HOKE spectroscopy[18] can be found if one knows population wave packets in the ground- and excited-electronic states (see eqs 2, 17, 18, and A9 below). These wave packets can be calculated by a nonperturbative analytic approach to the problem of the interaction of high-power chirped ultrashort pulses with molecular systems developed in ref 9 on the basis of the "moving potentials" picture. This approach has been generalized in ref 10 by inclusion of high-frequency quantum intramolecular modes. Nonperturbative equations for the populations of molecular electronic states under the action of intense chirped pulses have been obtained using the double-sided Feynman diagrams. All these consideration concerned Debye solvent. The relaxation in Debye solvent provides an example of a relaxation corresponding to a Markovian perturbation with the exponential correlation function. However, as recent studies show, the solvent relaxation is "biphasic": its correlation function typically consists of a fast (femtosecond) and a slower component.[26–31] The fastest component of solvent relaxation is typically a Gaussian (inertial) one. In addition, a fast component can correspond to a diffusive intramolecular vibrational mode. "Biphasic" relaxation and especially relaxation with the Gaussian fast component provide examples of relaxation corresponding to a *non-Markovian* random perturbation. Thus, if one wants to apply the technique in ref 10, for example, to a non-Debye solvent, one needs to include *non-Markovian* random perturbations. Here we generalize the theory of refs 9 and 10 to the relaxation in non-Debye solvent.

In ref 10, damping was included as a random perturbation by a Markovian process in the relevant electronic state. It is known that the equivalence exists between a

non-Markovian process and the suitable projection of an underlying multidimensional Markovian process.[32–35] Consequently, we can generalize the consideration of ref 10 to non-Markovian processes by using *multidimensional* Markovian processes. In the last case the double-sided Feynman diagrams for fast optical dephasing are similar to those of ref 10. The only difference is related to replacing the one-dimensional Liouville space Green functions by multidimensional ones. Summing the diagrams for a multidimensional Markovian processes similar to ref 10, we obtain the following equation for $\rho_{ns}(t)$:

$$\rho_{ns}(\{q\},\{p\},t) = \rho_{ns}^{(0)}(\{q\},\{p\}) + (-1)^n \frac{\pi}{2\hbar^2} \times \int_0^t dx |D\mathcal{E}(x)|^2 \int_{-\infty}^{\infty} d^k q' d^k p' \times \mathcal{G}_{nc}(\{q\},\{p\},\ t-x;\{q'\},\{p'\}) \times [F_{1M}(\omega(x) - \omega_{21}^{el} - V_s(\{q'\})/\hbar) \times \rho_{1s}(\{q'\},\{p'\},x) - F_{2M}(\omega(x) - \omega_{21}^{el} - V_s(\{q'\})/\hbar) \times \rho_{2s}(\{q'\},\{p'\},x)] \quad \text{(A1)}$$

for a *2k*-dimensional Markovian process. Here $\{p\}$ are momenta, $\{q\}$ are coordinates, $\rho_{ns}^{(0)}(\{q\},\{p\}) = \rho_{ns}(\{q\},\{p\},-\infty)$, $\mathcal{G}_{nc}(\{q\},\{p\},\ t-x;\{q'\},\{p'\})$ are the Liouville space Green functions,

$$F_{1,2M}(\omega') = \frac{1}{2\pi}\int_{-\infty}^{\infty} d\tau_1 f_{\alpha,\varphi M}(\tau_1)\exp(-i\omega'\tau_1) \quad \text{(A2)}$$

are the "intramolecular" (*M*) absorption (1) or luminescence (2) spectra of a solute molecule.

We assumed that $\mathcal{E}(x) \equiv 0$ for $-\infty < x \le 0$ when deriving eq A1. Equation A1 is a central result of the theoretical part of this work. It generalizes eq 37 of ref 10 to a non-Markovian random perturbation which can be represented by multidimensional Markovian processes.

Let us consider a special case of "biphasic" relaxation. We want to know how "biphasic" decay of the correlation function changes the dynamics of molecular optical transitions in the field of intense ultrashort chirped pulses. In a number of experimental works, an exponential fit was used for the fast component of the solvation correlation function.[36] Rigorous treatment of a biexponential correlation function is possible by the two-dimensional Markovian reaction-diffusion equation:[35] $L_{ns} = \sum_{j=1,2} L_{nsj} = \sum_{j=1,2} \tilde{D}_{nj}\frac{\partial}{\partial q_j}\left(\frac{\partial}{\partial q_j} + \beta\frac{\partial}{\partial q_j}U_{ns}(q_1,q_2)\right)$ where L_{ns} is the Fokker–Planck operator describing a diffusion in a two-dimensional potential $U_{ns}(q_1, q_2) = E_n + \frac{1}{2}\sum_{j=1,2}\omega_j^2(q_j - \delta_{n2}d_j)^2$. A differential equation for the quantity $\rho_{ns}(q_1, q_2, t)$ can be obtained similar to eq 42 of ref 10:

$$\left(\frac{\partial}{\partial t} - \tilde{L}_{ns}\right)\tilde{\rho}_{ns}(\alpha_1,\alpha_2,t) = (-1)^n \frac{\pi}{2\hbar^2}|D\mathcal{E}(t)|^2[F_{1M}(\omega(t) - \omega_{21} + \alpha_1 + \alpha_2) \times \tilde{\rho}_{1s}(\alpha_1,\alpha_2,t)\cdot F_{2M}(\omega(t) - \omega_{21} + \alpha_1 + \alpha_2) \times \tilde{\rho}_{2s}(\alpha_1,\alpha_2,t)] \quad \text{(A3)}$$

where $\omega_{21} = \omega_{21}^{el} + \omega_{st}/2$ is the frequency of the Franck–Condon transition $1 \rightarrow 2$ with respect to the configuration coordinates related to q_1 and q_2, $\omega_{st} = \sum_{j=1,2}\omega_{stj} = \sum_{j=1,2}\omega_j^2 d_j^2/\hbar$ is the contribution of the vibrations q_1 and q_2 to the Stokes shift of the equilibrium absorption and luminescence spectra,

$$\tilde{L}_{ns} = \sum_{j=1,2}\tilde{L}_{nsj} = \sum_{j=1,2}\tau_{snj}^{-1}\left[1 + (\alpha_j - \delta_{n2}\omega_{stj}) \times \frac{\partial}{\partial(\alpha_j - \delta_{n2}\omega_{stj})} + \sigma_{2sj}\frac{\partial^2}{\partial(\alpha_j - \delta_{n2}\omega_{stj})^2}\right] \quad \text{(A4)}$$

and $\tau_{snj} = \sigma_{2sj}/\tilde{D}_{nj}$ is the *j*th correlation time in state *n*. Here we introduced a new variable, $\alpha_j = q_j d_j \omega_j^2/\hbar$, so that $\rho_{ns}(q_1,q_2,t)dq_1dq_2 = \tilde{\rho}_{ns}(\alpha_1,\alpha_2,t)d\alpha_1 d\alpha_2$.

Solution of the two-dimensional Markovian reaction-diffusion equation, eq A3, is a much more complex problem than that of a one-dimensional equation. However, in order to take into consideration that, for a "biphasic" relaxation, the corresponding times differ greatly, the problem under consideration can be reduced to a one-dimensional one. Let us consider a frequently occurring situation where the duration of an ultrashort chirped pump pulse is of the same order of magnitude as that of the fastest relaxation component (q_1), but much shorter than the slow relaxation (q_2). Then eq A3 is reduced to

$$\left(\frac{\partial}{\partial t} - \tilde{L}_{ns1}\right)\tilde{\rho}_{ns}(\alpha_1,\alpha_2,t) = (-1)^n\frac{\pi}{2\hbar^2}|D\mathcal{E}(t)|^2 \times [F_{1M}(\omega(t) - \omega_{21} + \alpha_1 + \alpha_2)\tilde{\rho}_{1s}(\alpha_1,\alpha_2,t) - F_{2M}(\omega(t) - \omega_{21} + \alpha_1 + \alpha_2)\tilde{\rho}_{2s}(\alpha_1,\alpha_2,t)] \quad \text{(A5)}$$

Eq A5 is a one-dimensional diffusion equation depending parametrically on the slow coordinate α_2. It will be used for describing experimental results elsewhere.

Knowing the density matrix $\tilde{\rho}_{ns}(\alpha_1,\alpha_2,t)$, one can calculate the amplitude of the positive frequency component of the polarization $P^+(t)$ by generalization of equation 12 of ref 8 to a two-dimensional case

$$P^{+}(t) = \frac{iN|D_{12}|^2}{2\hbar}\mathcal{E}_{pr}(t-\tau) \times \int_{-\infty}^{\infty} d\alpha_1 \int_{-\infty}^{\infty} d\alpha_2 \int_{0}^{\infty} d\tau' \exp[i(\omega(t-\tau) - \omega_{21} + \alpha_1 + \alpha_2)\tau'] \times \{f^*_{\alpha M}(\tau')\tilde{\rho}_{1s}(\alpha_1,\alpha_2,t) - f^*_{\varphi M}(\tau')\tilde{\rho}_{2s}(\alpha_1,\alpha_2,t)\} \quad \text{(A6)}$$

Substituting the last equation into eq 4, we obtain for $\psi = 0$

$$J_{HOKE}(\tau) \sim -\frac{N|D_{12}|^2}{2\hbar}\int_{-\infty}^{\infty} dt|E_{LO}(t-\tau)|^2 \times \mathrm{Re}\int_{0}^{\infty} d\tau' \int_{-\infty}^{\infty} d\alpha_1 \int_{-\infty}^{\infty} d\alpha_2 \exp[i((\omega - \omega_{21} + \alpha_1 + \alpha_2)\tau' + \varphi(t-\tau-\tau'))]\{f^*_{\alpha M}(\tau')\tilde{\rho}^{NL}_{1s}(\alpha_1,\alpha_2,t) - f^*_{\varphi M}(\tau')\tilde{\rho}^{NL}_{2s}(\alpha_1,\alpha_2,t)\} \quad \text{(A7)}$$

where $\tilde{\rho}^{NL}_{ns}(\alpha_1,\alpha_2,t)$ is the deviations of $\tilde{\rho}_{ns}(\alpha_1,\alpha_2,t)$ from its equilibrium value

$$\tilde{\rho}^{(0)}_{ns}(\alpha_1,\alpha_2) = \delta_{n1}\prod_{i=1,2}(2\pi\sigma_{2si})^{-1/2}\exp[-\alpha_i^2/(2\sigma_{2si})] \quad \text{(A8)}$$

where $\sigma_{2si} = \omega_{sti}k_BT/\hbar$. For one normal intramolecular oscillator of frequency ω_0 whose characteristic functions are determined by eq 16, we obtain from eq A7

$$J_{HOKE}(\tau) \sim -\exp(-S_0\coth\theta_0) \times \sum_{k=-\infty}^{\infty} I_k(S_0/\sinh\theta_0)\exp(k\theta_0)\int_{-\infty}^{\infty} dt|\mathcal{E}_{LO}(t-\tau)|^2 \times \int_{-\infty}^{\infty} d\alpha_2 \{\tilde{\rho}^{NL}_{1s}[\omega_{21} - \omega(t-\tau) + k\omega_0 + \alpha_2, \alpha_2, t] - \tilde{\rho}^{NL}_{2s}[\omega_{21} - \omega(t-\tau) - k\omega_0 + \alpha_2, \alpha_2, t]\} \quad \text{(A9)}$$

REFERENCES AND NOTES

(1) Cerullo, G.; Bardeen, C.J.; Wang, Q.; Shank, C.V. *Chem. Phys. Lett.* **1996**, *262*, 362.
(2) Buist, A.H.; Müller, M.; Ghauhareli, R.I.; Brakenhoff, G. J.; Squier, J.A.; Bardeen, C.J.; Yakovlev, V.V.; Wilson, K.R. *Opt. Lett. 24*, 244.
(3) Fainberg, B.D.; Huppert, D.; Segal, J. In *Ultrafast Phenomena XII. Springer Series in Chemical Physics*; Elsaesser, T.; Mukamel, S.; Murnane, M.M.; Scherer, N.F., Eds.; Springer: Berlin, 2001; Vol. 66, pp 621–623.
(4) Fainberg, B.D. *Chem. Phys. Lett.* **2000**, *332*, 181.
(5) Sterling, M.; Zadoyan, R.; Apkarian, V.A. *J. Chem. Phys.* **1996**, *104*, 6497.
(6) Zadoyan, R.; Schwentner, N.; Apkarian, V.A. *Chem. Phys.* **1998**, *233*, 353.
(7) Bardeen, C.J.; Che, J.; Wilson, K.R.; Yakovlev, V.V.; Apkarian, V.A.; Martens, C.C.; Zadoyan, R.; Kohler, B.; Messina, M. *J. Chem. Phys.* **1997**, *106*, 8486.
(8) Fainberg, B.D.; Narbaev, V. *J. Chem. Phys.* **2002**, *116*, 4530.
(9) Fainberg, B.D. *J. Chem. Phys.* **1998**, *109*, 4523.
(10) Fainberg, B.D.; Narbaev, V. *J. Chem. Phys.* **2000**, *113*, 8113.
(11) Yan, Y.J.; Mukamel, S. *Phys. Rev. A* **1990**, *41*, 6485.
(12) Rosker, M.J.; Wise, F.W.; Tang, C.L. *Phys. Rev. Lett.* **1986**, 57, 321.
(13) Wise, F.W.; Rosker, M.J.; Tang, C.L. *J. Chem. Phys.* **1987**, *86*, 2827.
(14) Fainberg, B.D. *Chem. Phys.* **1990**, *148*, 33.
(15) Fainberg, B.D.; Zolotov, B.; Gan, A.; Goldberg, S.Y.; Huppert, D. In *Fast Elementary Processes in Chemical and Biological Systems. AIP Conf. Proc. 364*; Tramer, A., Ed.; AIP Press: Woodbury, NY, 1996; p 454.
(16) Zolotov, B.; Gan, A.; Fainberg, B.D.; Huppert, D. *Chem. Phys. Lett.* **1997**, *265*, 418.
(17) Zolotov, B.; Gan, A.; Fainberg, B.D.; Huppert, D. *J. Luminesc.* **1997**, *72–74*, 842.
(18) Fainberg, B.D.; Huppert, D. *Adv. Chem. Phys.* **1999**, *107* (*Chapter 3*), 191.
(19) Shen, Y.R. *The Principles of Nonlinear Optics*; John Wiley and Sons: New York, 1984.
(20) Lax, M. *J. Chem. Phys.* **1952**, *20*, 1752.
(21) Lin, S.H. *Theor. Chim. Acta* **1968**, *10*, 301.
(22) Abramowitz, M.; Stegun, I. *Handbook of Mathematical Functions*; Dover: New York, 1964.
(23) Martinez, O.E.; Gordon, J.P.; Fork, R. *J. Opt. Soc. Am.* **1984**, *A 1*, 1003.
(24) Armstrong, J.A. *Appl. Phys. Lett.* **1967**, *10*, 16.
(25) Kosloff, R.; Tal-Ezer, H. *Chem. Phys. Lett.* **1986**, *127*, 223.
(26) Rosenthal, S.J.; Xiaoliang, X.; Du, M.; Fleming, G.R. *J. Chem. Phys.* **1991**, *95*, 4715.
(27) Cho, M.; Rosenthal, S.J.; Scherer, N.F.; Ziegler, L.D.; Fleming, G.R. *J. Chem. Phys.* **1992**, *96*, 5033.
(28) Rosenthal, S.J.; Jimenez, R.; Fleming, G.R.; Kumar, P.V.; Maroncelli, M. *J. Mol. Liq.* **1994**, *60*, 25.
(29) Bagchi, B.; Chandra, A. *J. Chem. Phys.* **1992**, *97*, 5126.
(30) Neria, E.; Nitzan, A. *J. Chem. Phys.* **1992**, *96*, 5433.
(31) Jimenez, R.; Fleming, G.R.; Kumar, P.V.; Maroncelli, M. *Nature* **1994**, *369*, 471.
(32) Rytov, S.M. *Introduction to the Statistical Radiophysics*; Nauka: Moscow, 1976 (in Russian).
(33) Risken, H. *The Fokker-Planck Equation*; Springer-Verlag: Berlin, 1984.
(34) Bicout, D.J.; Szabo, A. *J. Chem. Phys.* **1998**, *108*, 5491.
(35) Bicout, D.J.; Szabo, A. *J. Chem. Phys.* **1998**, 109, 2325.
(36) Horng, M.L.; Gardecki, J.; Papazyan, A.; Maroncelli, M. *J. Phys. Chem.* **1995** *99*, 17311.
(37) Huang, K.; Rhys, A. *Proc. R. Soc. London* **1950**, *A204*, 406.